Science of the Total Environment 820 (2022) 153153

Contents lists available at ScienceDirect

Science of the Total Environment

journal homepage: www.elsevier.com/locate/scitotenv

Mechanisms of orthophosphate removal from water by lanthanum carbonate and other lanthanum-containing materials

Yue Zhi [a,b,*], Alisa R. Paterson [c], Douglas F. Call [b], Jacob L. Jones [c], Dean Hesterberg [d], Owen W. Duckworth [d], Eric P. Poitras [e], Detlef R.U. Knappe [b]

[a] Key Laboratory of Eco-environments in Three Gorges Reservoir Region, Ministry of Education, College of Environment and Ecology, Chongqing University, Chongqing 400044, China
[b] Department of Civil, Construction, and Environmental Engineering, North Carolina State University, Raleigh, NC 27695, USA
[c] Department of Materials Science and Engineering, North Carolina State University, 27695, Raleigh, NC, USA
[d] Department of Crop and Soil Sciences, North Carolina State University, 27695 Raleigh, NC, USA
[e] Analytical Sciences Department, Research Triangle Institute, 27709 Durham, NC, USA

HIGHLIGHTS

- We studied mechanisms of PO_4 removal by $La_2(CO_3)_3$ and other La-containing materials.
- PO_4 removal occurred primarily by precipitation of $LaPO_4$.
- PO_4 removal rates increased with decreasing solution pH.
- $La_2(CO_3)_3$ selectively removed PO_4 from wastewater.
- Low solubility of $La_2(CO_3)_{3(s)}$ minimizes release of soluble La into the environment.

GRAPHICAL ABSTRACT

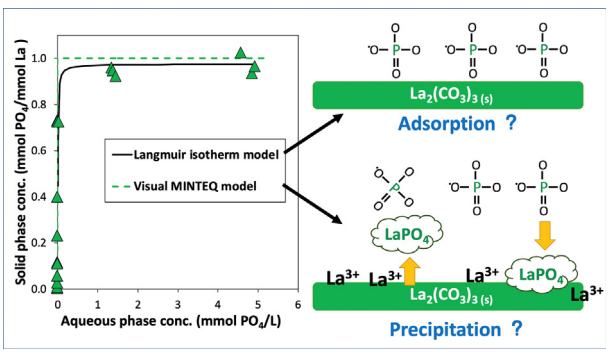

ARTICLE INFO

Article history:
Received 19 October 2021
Received in revised form 19 December 2021
Accepted 11 January 2022
Available online 15 January 2022

Editor: Yifeng Zhang

Keywords:
Lanthanum containing material
Lanthanum carbonate
Phosphorus removal
Wastewater treatment
Mineral precipitation

ABSTRACT

Removing phosphorus (P) from water and wastewater is essential for preventing eutrophication and protecting environmental quality. Lanthanum [La(III)]-containing materials can effectively and selectively remove orthophosphate (PO_4) from aqueous systems, but there remains a need to better understand the underlying mechanism of PO_4 removal. Our objectives were to 1) identify the mechanism of PO_4 removal by La-containing materials and 2) evaluate the ability of a new material, $La_2(CO_3)_{3(s)}$, to remove PO_4 from different aqueous matrices, including municipal wastewater. We determined the dominant mechanism of PO_4 removal by comparing geochemical simulations with equilibrium data from batch experiments and analyzing reaction products by X-ray diffraction and scanning transmission electron microscopy with energy dispersive spectroscopy. Geochemical simulations of aqueous systems containing PO_4 and La-containing materials predicted that PO_4 removal occurs via precipitation of poorly soluble $LaPO_{4(s)}$. Results from batch experiments agreed with those obtained from geochemical simulations, and mineralogical characterization of the reaction products were consistent with PO_4 removal occurring primarily by precipitation of $LaPO_{4(s)}$. Between pH 1.5 and 12.9, $La_2(CO_3)_{3(s)}$ selectively removed PO_4 over other anions from different aqueous matrices, including treated wastewater. However, the rate of PO_4 removal decreased with increasing solution pH. In comparison to other solids, such as $La(OH)_{3(s)}$, $La_2(CO_3)_{3(s)}$ exhibits a relatively low solubility, particularly under slightly acidic conditions. Consequently, release of La^{3+} into the environment can be minimized when $La_2(CO_3)_{3(s)}$ is deployed for PO_4 sequestration.

* Corresponding author at: Key Laboratory of Eco-environments in Three Gorges Reservoir Region, Ministry of Education, College of Environment and Ecology, Chongqing University, Chongqing 400044, China.
E-mail address: yuezhi6170@163.com (Y. Zhi).

http://dx.doi.org/10.1016/j.scitotenv.2022.153153

1. Introduction

Phosphorus (P) is a critical, nonrenewable resource that is essential for global food production. Excessive P discharge to aquatic ecosystems is not only wasteful but can also cause eutrophication and harmful algal blooms, diminishing water quality and potentially threatening wildlife and human health (Conley et al., 2009; Mayer et al., 2016). In aquatic environments, P can exist in a variety of forms, including orthophosphate (PO_4, including H_3PO_4, $H_2PO_4^-$ and HPO_4^{2-}, and PO_4^{3-}), polyphosphate, and organic P. Orthophosphate is the form that is most readily assimilated by plants and is therefore the target of many efforts to remove and recover P from water (Weiner, 2008).

One approach to capture P from water is to develop materials that have a high affinity for PO_4. In this context, lanthanum (La)-containing materials are receiving considerable attention (Zhi et al., 2020). Materials that have been tested include La-modified (alumino)silicates (Copetti et al., 2016; Douglas, 2002; Douglas et al., 1999; Huang et al., 2015; Huang et al., 2014b; Lai et al., 2016; Reitzel et al., 2013; Robb et al., 2003; Waajen et al., 2016; Xie et al., 2014; Yang et al., 2011, 2012; Zhang et al., 2011), carbonaceous materials (e.g., graphene, activated carbon fiber, biochar) (Chen et al., 2016; Liu et al., 2011; Rashidi Nodeh et al., 2017; Shin et al., 2005; Zhang et al., 2012b), polymers (Dong et al., 2017; He et al., 2015; Wu et al., 2007; Zhang et al., 2016), iron oxides (Fang et al., 2018; Lai et al., 2016; Wu et al., 2017), and aluminum hydroxide (Xu et al., 2017). La-containing materials exhibit remarkable PO_4 removal capacities (up to 2.91 mmol PO_4 g^{-1} estimated from Langmuir model fits to isotherm data, Dong et al., 2017) across a wide pH range (2.5–11) (Dong et al., 2017; Xie et al., 2014). Additionally, La-containing materials possess high selectivity for PO_4 anions in the presence of competing anions and ligands (e.g., Cl^-, NO_3^-, F^-, SO_4^{2-}, SO_3^{2-}, HCO_3^-, SiO_4^{4-}, and Br^-), even when molar concentrations of competing ions exceeded that of PO_4 by up to 50 times (Chen et al., 2016; Dong et al., 2017; Huang et al., 2014a; Rashidi Nodeh et al., 2017; Wu et al., 2007, 2017; Zhang et al., 2011, 2016). Phosphate capture efficiency is also high in complex aqueous matrices such as surface water (Dithmer et al., 2016; Reitzel et al., 2013; Waajen et al., 2016), seawater (Mucci et al., 2020; Wu et al., 2007), wastewater (Wu et al., 2007), and brackish water (Reitzel et al., 2013). The high affinity of La-containing materials for PO_4 has been confirmed in short- and long-term laboratory-, mesocosm-, and field-scale studies (Dithmer et al., 2016; Waajen et al., 2016). As a result, commercially-available products, such as La-modified bentonite clay (Phoslock®), have been developed for PO_4 sequestration (Copetti et al., 2016).

Although La-containing materials have been widely studied, there are conflicting reports about the underlying PO_4 removal mechanism. In peer-reviewed articles, most previous studies concluded that removal of PO_4 is an adsorption phenomenon (Table S1) (Chen et al., 2016, 2018; Cheng et al., 2018; Dong et al., 2017; Du et al., 2018; Emmanuelawati et al., 2013; Fang et al., 2018; Huang et al., 2014a; Huang et al., 2014b; Huang et al., 2015; Jia et al., 2019; Kong et al., 2018; Lai et al., 2016; Lin et al., 2019; Liu et al., 2011, 2013; Rashidi Nodeh et al., 2017; Shin et al., 2005; Tang et al., 2019; Wu et al., 2017; Wu et al., 2019b; Xie et al., 2014; Xu et al., 2017; Yang et al., 2011, 2012; Yu et al., 2019; Yuan et al., 2018; Zhang et al., 2011, 2012a, 2016, 2018). Evidence is often provided by describing data from batch tests with adsorption isotherm models; however, such an approach cannot differentiate between adsorption and other removal mechanisms (Sposito, 2004). For example, Veith and Sposito showed that the Langmuir isotherm model (Eq. S1), which is a classic adsorption model, could describe equally well both adsorption and precipitation phenomena (Veith and Sposito, 1977). It has been speculated that mechanisms of PO_4 adsorption by $La(OH)_{3(s)}$ or $La_2O_3{\cdot}xH_2O_{(s)}$ include electrostatic interactions (Dong et al., 2017; Wu et al., 2017), ion exchange (Park et al., 2020; Xie et al., 2014), ligand exchange (Dong et al., 2017; Fang et al., 2017; Wu et al., 2017, 2019a, 2019b; Xie et al., 2014; Xu et al., 2017; Zhang et al., 2012b), and Lewis acid-base interactions (Huang, 2011; Zhang et al., 2012b). However, some studies have attributed PO_4 removal by La-containing materials, such as La^{3+} or $La(OH)_{3(s)}$, to $LaPO_{4(s)}$ precipitation (Dithmer et al., 2015; He et al., 2015; Qiu et al., 2017), lending uncertainty to the dominant mechanism of PO_4 removal by La-containing materials.

One concern about La-containing materials is their dissolution, potentially leading to the release of La^{3+} into the environment (Copetti et al., 2016; Reitzel et al., 2017; Zhi et al., 2021). Dissolution of La was observed in previous studies, especially at low pH (pH < 4.5–5.6) (Shin et al., 2005; Wu et al., 2017) or under high salinity (Douglas et al., 2000). Among aqueous La species (e.g., La^{3+} and $LaOH^{2+}$), La^{3+} is considered to be the most toxic (Das et al., 1988). However, no regulatory standards for La concentrations and discharges to the environment have been set because of a lack of risk characterization data. A predicted no effect concentration (PNEC) based on *Daphnia carinata* assays (Barry and Meehan, 2000) of 4 μg L^{-1} (2.9×10^{-8} M) has been proposed as a water quality criterion (Herrmann et al., 2016). Additionally, introducing soluble La species into aquatic environments may lead to a range of ecotoxicological effects (Copetti et al., 2016; Gonzalez et al., 2014). Despite the potential risks, La dissolution data from solids designed for PO_4 removal are scarce, and few comparisons across different La-containing materials have been made (Wu et al., 2019a, 2019b; Zhi et al., 2020, 2021).

Objectives of our research were to 1) determine the mechanism of PO_4 removal by La-containing materials and 2) evaluate the effectiveness of a new material, $La_2(CO_3)_{3(s)}$, for PO_4-removal from complex aqueous matrices, including wastewater effluent. We selected $La_2(CO_3)_{3(s)}$ because it is less soluble at circumneutral pH than other La-containing salts (Table S5) (Gustafsson, 2011), and thus we hypothesized that $La_2(CO_3)_{3(s)}$ would enable PO_4 removal without significant release of La to the aqueous phase. We conducted batch experiments, geochemical simulations, and solid-phase characterizations to: (1) compare the stability of $La_2(CO_3)_{3(s)}$ and $La(OH)_{3(s)}$ in pure water and municipal wastewater as a function of solution pH; (2) identify the dominant mechanism of PO_4 removal; and (3) assess the selectivity of $La_2(CO_3)_{3(s)}$ for PO_4 in wastewater effluent. We characterized starting materials and reaction products by X-ray diffraction (XRD) and scanning transmission electron microscopy with energy dispersive spectroscopy (STEM-EDS) analysis to provide insights into the dominant mechanism of PO_4 removal.

2. Materials and methods

2.1. Materials

Experiments were conducted using $La_2(CO_3)_3{\cdot}8H_2O_{(s)}$ (99.99%, Alfa Aesar, Thermo Fisher Scientific MA, USA), $La(OH)_{3(s)}$ (99.9%), and $LaCl_3{\cdot}7H_2O$ (64.5–70.0%, $LaCl_3$ basis, both from Sigma-Aldrich). Sodium phosphate monobasic monohydrate, NaOH (1 N) and HCl (1 N) were supplied by Fisher Scientific (NH, USA). Tertiary-treated municipal wastewater was collected from a local wastewater treatment plant. The wastewater sample was filtered through a series of glass fiber and polyvinylidene fluoride (PVDF) membrane filters (down to 0.1 μm PVDF) prior to use. Wastewater composition data are available in the Supporting Information (Table S2).

2.2. Material characterization

Zeta potential and size distribution of $La_2(CO_3)_{3(s)}$ particles were measured in pH-adjusted (pH 5.8–12.6) suspensions (1 g L^{-1}) in ultrapure water (UPW) using dynamic light scattering (DLS, Zetasizer Nano ZS, Malvern Instruments Ltd.). Brunauer, Emmett, and Teller (BET) surface area was determined by N_2 gas adsorption (Autosorb IQ-MP/XR, Quantachrome Instruments, FL, USA). The morphologies of $La_2(CO_3)_{3(s)}$ and products formed after contact with PO_4 were determined by scanning transmission electron microscopy (STEM) on a Titan 60–300 G2 microscope (FEI) equipped with a dedicated energy dispersive spectroscopy (EDS) detector (SuperX), using an acceleration voltage of 200 kV. X-ray diffraction (XRD) measurements were performed using Cu K_α radiation (PANalytical Empyrean X-ray diffractometer equipped with a PIXcel1D

detector, Almelo, Netherlands) at a 2θ range of 5–70°, using a step size of 0.01° and a count time of 200 s/step. Phase identification was done using the software HighScore Plus 3.0e (PANalytical B.V., Almelo, Netherlands).

2.3. Analysis of aqueous species

Major ions in wastewater were analyzed using ion chromatography (IC, Dionex ICS-6000 and ICS-2000, Thermo Scientific) with a detection limit of 0.5 mg L^{-1} for all ions. Trace metals, including La^{3+}, were measured by inductively coupled plasma optical emission spectrometry (ICP-OES, iCAP 7600, Thermo, Bremen, Germany). The detection limit for La was 0.025 mg L^{-1}. Concentrations of dissolved PO_4 between 1 and 100 mg PO_4 L^{-1} were analyzed with the molybdovanadate method (Hach High range reactive phosphorus Test'N Tube vials with a Hach DR500 spectrometer). Samples containing <1 mg PO_4 L^{-1} were analyzed by ICP-OES with a reporting limit of 0.025 mg L^{-1}.

2.4. Batch experiments

The same general procedures were used for both batch kinetic and equilibrium experiments to evaluate PO_4 removal as a function of pH. Phosphate solutions were prepared by dissolving $NaH_2PO_4 \cdot H_2O$ in CO_2-free UPW. The initial pH was adjusted to target values for the experiment with 1 N solutions of NaOH or HCl. The volume of acid/base added was <1% (v/v) of each experiment. Experiments evaluating PO_4 uptake between pH 0.4 and 12.5 were performed as follows: 1) 0.100 g of $La_2(CO_3)_3 \cdot 8H_2O_{(s)}$ (3.23 mM La) was added to 100.0 mL of phosphate solution (initial PO_4 concentration: 1.62 mM) in HDPE bottles; 2) the bottles were capped immediately and shaken horizontally on a reciprocating shaker at 250 rpm and 25 °C from 1 to 44 days; 3) at each sampling time, an aliquot was collected from each bottle and centrifuged at 31,000 relative centrifugal force (RCF) for 20 min and the supernatant filtered (0.2 μm, PVDF membrane) before analysis; and 4) the pH of the remaining suspension was measured and adjusted back to the target pH ($\Delta pH < 0.1$ when pH = 4 or > 10, ΔpH = 0.01–0.8 prior to adjustment at pH 7 and pH 8.5) after each sampling. Our results show that ΔpH of 0.01–0.8 is negligible in shifting the dissolution of $La_2(CO_3)_3 \cdot 8H_2O_{(s)}$. (Figs. 1a and 2b).

In equilibrium experiments, 0.050 g of $La_2(CO_3)_3 \cdot 8H_2O_{(s)}$ (3.23 mM of La) was added to 50.0 mL of phosphate solution with an initial concentration from 1 to 800 mg PO_4 L^{-1} (0.01–8.42 mM) in polypropylene centrifuge tubes. Samples were equilibrated on a platform shaker at 25 °C for 2–3 days beyond the equilibrium time established in prior kinetic experiments. Detailed contact time information is given in Table S3. To compare the performance of different La-containing materials, equilibrium experiments were conducted with $La_2(CO_3)_{3(s)}$ and $LaCl_3$. The dosage of La was identical (3.23 mM La) in all systems. To evaluate the selectivity of $La_2(CO_3)_{3(s)}$ for PO_4, kinetic and equilibrium experiments were carried out in tertiary-treated wastewater in the same manner as in UPW. The raw PO_4 concentration in the wastewater was low (0.3 mg PO_4 L^{-1}, Table S2), so PO_4 was added to reach a working concentration equivalent to the UPW experiments (1.62 mM, 153 mg PO_4 L^{-1}).

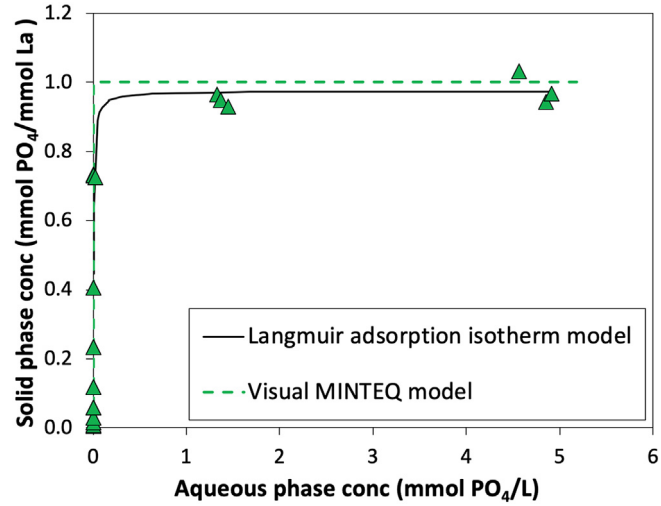

Fig. 2. Equilibrium data (green triangles) describing PO_4 association with a solid phase following addition of $La_2(CO_3)_{3(s)}$ (starting PO_4 concentrations: 0.01–8.42 mM, $La_2(CO_3)_{3(s)}$ dose: 1.62 mM, experimental conditions: UPW, pH 7, 25 °C). Visual MINTEQ results indicating $LaPO_{4(s)}$ precipitation and the best fit of the Langmuir isotherm model are shown as dotted and solid lines, respectively. Visual MINTEQ was executed by sweeping PO_4 concentrations from 0.01–8.42 mM at pH 7 and 25 °C. Model inputs included 1.62 mM of $La_2(CO_3)_{3(s)}$ as finite solid, $La(OH)_{3(s)}$ and $LaPO_{4(s)}$ as possible solids. Detailed model inputs and equilibrium constants are listed in Tables S4-S5.

2.5. Chemical equilibrium modeling

The chemical equilibrium model Visual MINTEQ (version 3.1) was used to simulate the stability of La-containing materials and their interactions with PO_4 under varying pH and ionic conditions relevant to our samples.

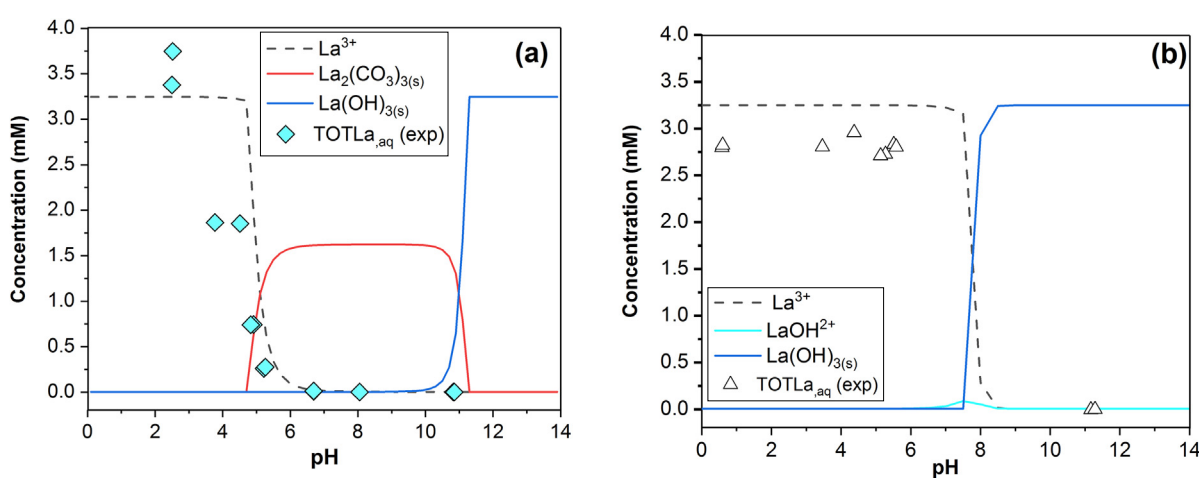

Fig. 1. Speciation of aqueous and solid La following addition of (a) 1.62 mM $La_2(CO_3)_{3(s)}$ or (b) 3.25 mM $La(OH)_{3(s)}$ to UPW at 25 °C. Lines represent Visual MINTEQ results and symbols data from batch experiments. $TOTLa_{(aq)}$ – total aqueous La. Visual MINTEQ was executed for each condition by sweeping pH from 0 to 14 at 25 °C. Model inputs included (a) 1.62 mM of $La_2(CO_3)_{3(s)}$ as a finite solid and $La(OH)_{3(s)}$ as possible solid or (b) 3.25 mM of $La(OH)_{3(s)}$ as a finite solid. Detailed model inputs and equilibrium constants are listed in Tables S4-S5.

Underlying model assumptions were: 1) aqueous equilibrium is established; possible solids precipitate such that no supersaturated species are present at equilibrium; and 2) the system is closed and at 25 °C. Model inputs and solubility product constants are listed in Tables S4-S5. Visual MINTEQ was executed for each condition by sweeping pH and model predictions were validated by batch experimental and spectroscopic data.

3. Results and discussion

3.1. Surface properties and chemical stability of La solids

The zeta potential of $La_2(CO_3)_{3(s)}$ varied from 38.6 mV at pH 6 to a minimum of −47.2 mV at pH 11 (Fig. S1). The isoelectric point (IEP) was at pH 8.5, which is within the range of metal carbonates (5.8–9.0) (Pokrovsky and Schott, 2002). The IEP value is higher than that reported for materials modified with $La(OH)_3/La_2O_{3(s)}$ (5.2–5.8) (Chen et al., 2016; Wu et al., 2017), but lower than that reported for pure La_2O_3(s) (9.6) (Roy and Sengupta, 1988). The hydrodynamic diameter of particles measured by DLS was 1400 ± 70 nm at the point of zero charge (PZC), and 307 ± 41 nm above or below the PZC (Fig. S1). The Brunauer, Emmett, and Teller (BET) surface area of $La_2(CO_3)_{3(s)}$ was 5.2 $m^2\,g^{-1}$ as determined from nitrogen (N_2) adsorption data.

To compare the stability of La solids, dissolution of $La_2(CO_3)_{3(s)}$ and precipitation of La^{3+} as $La(OH)_{3(s)}$ in the absence of PO_4 was assessed as a function of pH both experimentally and through geochemical equilibrium simulations. Following equilibration of $La_2(CO_3)_{3(s)}$ or $La(OH)_{3(s)}$ (3.23 mM La) in UPW, total aqueous La concentrations ($TOTLa_{(aq)}$) determined in batch experiments were consistent with model simulations (Fig. 1). For $La_2(CO_3)_{3(s)}$, ≥90% of the added La was predicted to remain as $La_2(CO_3)_{3(s)}$ between pH 5.5 and 10.7. At pH <5.5, La^{3+} increased, and at pH >10, $La_2(CO_3)_{3(s)}$ was predicted to convert to $La(OH)_{3(s)}$ (Fig. 1a).

For $La(OH)_{3(s)}$, ≥90% of the added La was predicted to remain as $La(OH)_{3(s)}$ at pH >8, while at pH <7.5, >90% of $La(OH)_{3(s)}$ dissolved (Fig. 1b). Over the environmentally relevant pH range of 6.0–8.5, $TOTLa_{(aq)}$ in equilibrium with $La_2(CO_3)_{3(s)}$, ranged from 9.5×10^{-5} M at pH 6 to 1.7×10^{-6} M at pH 8.5. This range was 1–2 orders of magnitude lower than that in equilibrium with $La(OH)_{3(s)}$, which ranged from 3.2×10^{-3} M at pH 6 to 1.3×10^{-5} M at pH 8.5 (logarithmic results shown in Fig. S2a).

3.2. PO_4 removal by $La_2(CO_3)_{3(s)}$ at pH 7

To evaluate PO_4-removal by $La_2(CO_3)_{3(s)}$, equilibrium experiments with varying initial PO_4 concentrations (0.01–8.42 mM) and a fixed concentration of $La_2(CO_3)_{3(s)}$ (3.23 mM La) were conducted in UPW at pH 7. Based on prior studies suggesting that adsorption drives the removal of PO_4 on La-containing materials and our equilibrium model predictions that $La_2(CO_3)_{3(s)}$ is a stable solid at pH 7 (Fig. 1a), we fit the data of equilibrium experiments with the Langmuir isotherm model (Eq. S1). This model provides a good fit to the data (Fig. 2, with Langmuir isotherm model parameters given in Table S6). However, it is worth noting that the sorption maxima in Fig. 2 translate to a theoretical surface loading of about 500 PO_4 anions nm^{-2}, a physically unrealistic number that exceeds by >200-fold estimates of typical surface site densities of minerals (2.3 sites nm^{-2}) (Davis, 1990; Dzombak and Morel, 1990; Field et al., 2019).

Alternatively, previous studies have suggested that PO_4 removal by La-containing materials occurs by precipitation (Dithmer et al., 2015; Douglas et al., 2000; He et al., 2015; Qiu et al., 2017; Slade and Gates, 1999). Equilibrium solubility calculations conducted in Visual MINTEQ can be used to predict soluble PO_4 concentrations observed in our batch tests (Fig. 2). Visual MINTEQ predicted that precipitation of $LaPO_{4(s)}$ would occur, and model results effectively described the batch equilibrium data shown in Fig. 2.

Importantly, our data in Fig. 2 approach a 1:1 M ratio of P:La in the solid phase once the molar PO_4 concentration exceeded the molar La concentration. This result is indicative of the formation of a solid with a 1:1 stoichiometry, consistent with the precipitation of $LaPO_4$ or one of its hydrated forms. Interestingly, a re-evaluation of previously published data (n = 35, including studies that describe PO_4 removal as an adsorption phenomenon (Chen et al., 2016, 2018; Cheng et al., 2018; Dong et al., 2017; Du et al., 2018; Emmanuelawati et al., 2013; Fang et al., 2018; Huang et al., 2014a; Huang et al., 2014b; Huang et al., 2015; Jia et al., 2019; Kong et al., 2018; Lai et al., 2016; Lin et al., 2019; Liu et al., 2011, 2013; Rashidi Nodeh et al., 2017; Shin et al., 2005; Tang et al., 2019; Wu et al., 2017; Wu et al., 2019b; Xie et al., 2014; Xu et al., 2017; Yang et al., 2011, 2012; Yu et al., 2019; Yuan et al., 2018; Zhang et al., 2011, 2012a, 2016, 2018)) reveals a 1:1 stoichiometry of P removal by La-containing materials (Table S1).

PO_4 uptake, on a molar basis, when plotted against the molar La content of the studied materials [La^{3+}, $La_2(CO_3)_{3(s)}$, or $La(OH)_{3(s)}$-containing] largely describes a 1:1 line, consistent with the stoichiometry of $LaPO_{4(s)}$ (Fig. S3a). This result would require every La atom to bind a PO_4, a conceptual model that is not consistent with adsorption to a mineral surface. It is worth noting that maximum PO_4 adsorption by a diverse range of iron-bearing phases found variable and much lower molar ratios of P:Fe (0.3 to 0.02) (Rentz et al., 2009), further highlighting that the 1:1 stoichiometry observed for the La-containing materials differs from that expected for adsorption. Although deviations from the 1:1 stoichiometric ratio for La-containing materials in Fig. S3a could indicate other mechanisms, it may also reflect experimental differences such as contact time (some studies used contact times as short as 25 min (Chen et al., 2016), while others did not report contact time), carrier materials with intrinsic P-binding capacity (e.g. iron oxides (Wu et al., 2017)). Furthermore, PO_4 removal was independent of the specific surface of the starting material (Fig. S3b), which would be expected to be an important control on sorption maxima if adsorption were the dominant removal mechanism (Field et al., 2019; Sowers et al., 2017). Overall, observations of reaction stoichiometry in Figs. 2 and S3 suggest that PO_4 removal by La-containing materials occurs by precipitation, although additional solid phase characterization (*vida infra*) is required to document the presence of $LaPO_{4(s)}$ precipitates (see Section 3.4).

3.3. pH-dependent PO_4 removal by aqueous La^{3+} and $La_2(CO_3)_{3(s)}$

We next explored PO_4 removal by $La_2(CO_3)_{3(s)}$ over a wider pH range (0–14) (Fig. 3a). In the presence of $La_2(CO_3)_{3(s)}$, the geochemical equilibrium model predicted that PO_4 precipitates as $LaPO_{4(s)}$ between pH 1.0 and 13.5, with low $TOTPO_{4(aq)}$ that increases below and above this pH range (Fig. 3a). For pH < 10, experimental results were in agreement with Visual MINTEQ predictions for the sum of all aqueous PO_4 species ($TOTPO_{4(aq)}$) and $TOTLa_{(aq)}$.

Measured $TOTPO_{4(aq)}$ between pH 10 and 12 (after 168 h of contact) did not agree with Visual MINTEQ predictions. To determine if the discrepancy was attributable to non-equilibrium conditions, we conducted an additional experiment for 1048 h at pH 12 (dark blue circles in Fig. 3a). At the end of that experiment, $TOTPO_{4(aq)}$ was in close agreement with the Visual MINTEQ prediction (Fig. 3a). The latter result indicates that 168 h was insufficient to establish equilibrium at pH > 10. To further verify Visual MINTEQ predictions, we initially reacted PO_4 with $La_2(CO_3)_{3(s)}$ for 120 h without pH control (initial pH ~5, final pH ~7, Fig. S4), at which point $TOTPO_{4(aq)}$ decreased to below detection; then, the solution pH was adjusted to 12 to test if $TOTPO_{4(aq)}$ would increase (i.e., $LaPO_{4(s)}$ dissolution). Following base addition, no PO_4 was released to solution, even after 1048 h (Fig. S4), which further validated equilibrium model results (Fig. 3a).

Additionally, our experimental $TOTLa_{(aq)}$ concentrations were consistent with Visual MINTEQ equilibrium calculations (Fig. 3b). It is worth noting that calculations predicted that: 1) between pH 0.5 and 4, PO_4 addition stoichiometrically converted aqueous La^{3+} released from $La_2(CO_3)_{3(s)}$ to $LaPO_{4(s)}$; 2) between pH 5.5 and 11, $La_2(CO_3)_{3(s)}$ and $LaPO_{4(s)}$ co-existed and controlled La solubility; 3) between pH 11 and 13.5, $La(OH)_{3(s)}$ and $LaPO_{4(s)}$ co-existed and controlled La solubility; and 4) at pH >13.5, $La(OH)_{3(s)}$ controlled La solubility and $LaPO_4$ dissolved (Fig. 3b).

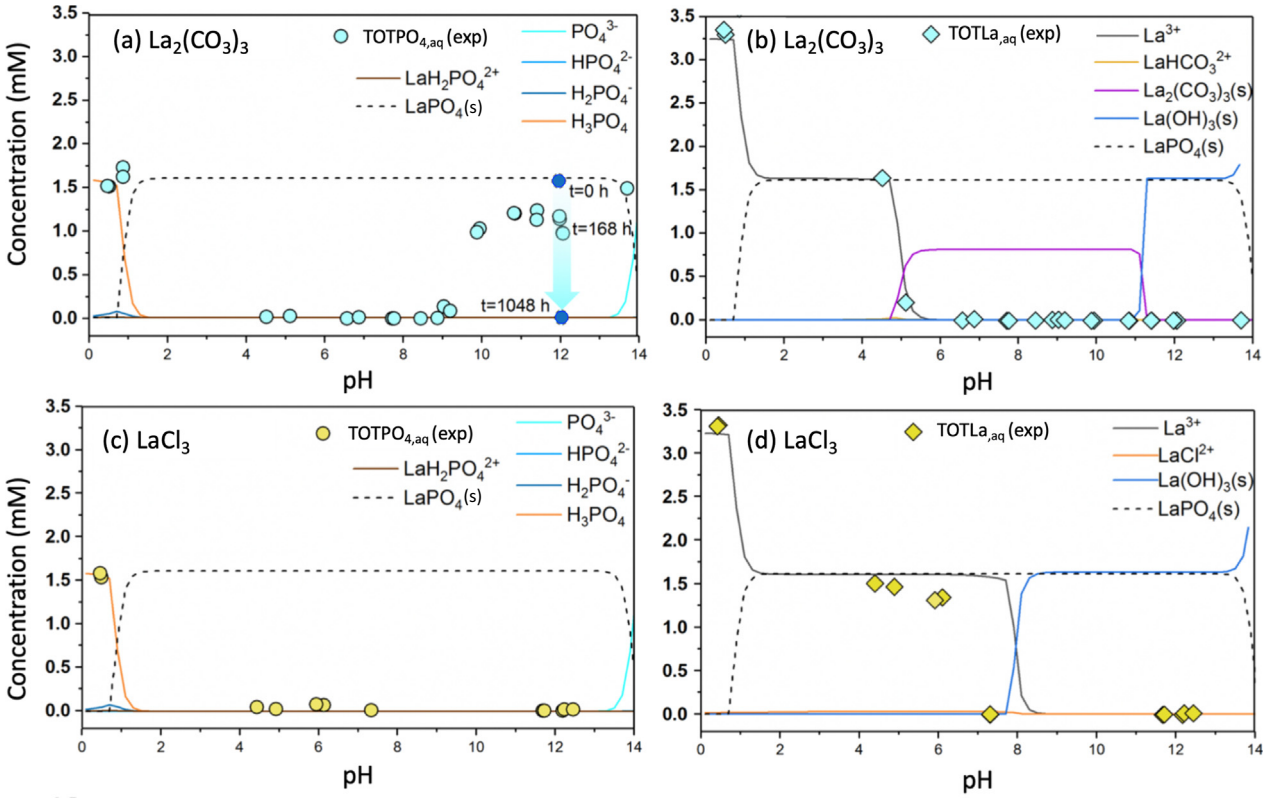

Fig. 3. Solution pH-dependent equilibrium concentrations of PO_4 and La species following addition of 1.62 mM $La_2(CO_3)_{3(s)}$ (panels a and b) or 3.23 mM $LaCl_3$ (panels c and d) to reactors containing 1.62 mM NaH_2PO_4 at 25 °C (La:*P* = 2:1). Lines: Visual MINTEQ results, symbols: experimental data. Equilibration time: 168 h, except dark-blue points and arrow in (a), which show a decline in PO_4 between 0 and 1048 h at pH 12. Only species with concentrations $>10^{-3}$ mM are shown. Visual MINTEQ was executed for each condition by sweeping pH from 0 to 14 at 5 °C. Model inputs for panels a and b include 1.62 mM of $La_2(CO_3)_{3(s)}$ as finite solid, and $La(OH)_{3(s)}$ and $LaPO_{4(s)}$ as possible solids; 1.62 mM of PO_4 and 1.62 mM of Na. Model inputs for panels c and d include 1.62 mM of PO_4, 1.62 mM of Na, and 3.23 mM of La; and $La_2(CO_3)_{3(s)}$, $La(OH)_{3(s)}$ and $LaPO_{4(s)}$ as possible solids. More details on model inputs and equilibrium constants are listed in Tables S4-S5.

We also conducted experiments with $LaCl_3$, a salt that is soluble at pH <7.5, thus not precipitating to provide surfaces for adsorption (Fig. 1b). In Fig. 3c, measured $TOTPO_{4(aq)}$ between pH 0.3 and 12.6 was similar to the corresponding $La_2(CO_3)_{3(s)}$ system and consistent with model predictions of $LaPO_{4(s)}$ precipitation. In Fig. 3d, a decrease in the experimentally determined $TOTLa_{(aq)}$ between pH 6 and 12 suggests that excess La (molar P:La = 1:2 in our experiments) precipitated as $La(OH)_{3(s)}$ and co-existed with $LaPO_{4(s)}$, consistent with the thermodynamic prediction of both solids co-existing at pH ≥ 8. In the presence of PO_4, $TOTLa_{(aq)}$ was three orders of magnitude lower over the environmentally relevant pH range of 6.0–8.5 in the system containing $La_2(CO_3)_{3(s)}$ (2.0×10^{-6} M - 1.4×10^{-8} M) than in the system containing $La^{3+}/La(OH)_{3(s)}$ (1.6×10^{-3} - 1.7×10^{-5} M) (Fig. S2b). This result indicates a lower potential for La dissolution in systems containing $La_2(CO_3)_{3(s)}$ at environmentally relevant pH.

3.4. Direct evidence of $LaPO_{4(s)}$ formation

Results from batch tests and Visual MINTEQ suggest PO_4 removal by La-containing materials occurs by formation of $LaPO_4$ precipitate. To provide evidence of $LaPO_{4(s)}$ precipitation, samples from batch equilibrium experiments were analyzed by XRD to identify solid phases formed during reaction with PO_4. The XRD pattern of the $La_2(CO_3)_3{\cdot}8H_2O_{(s)}$ starting material (Fig. 4, trace a) was compared to XRD patterns of the products after $La_2(CO_3)_{3(s)}$ reacted with PO_4 (molar P:La = 1:2) in UPW at pH 7 and pH 12, as well as in wastewater (Fig. 4, traces b-d; see also Section 3.6). Phase identification of the peaks in Fig. 4, traces b-d confirmed the presence of both $La_2(CO_3)_3{\cdot}8H_2O_{(s)}$ and $LaPO_4{\cdot}nH_2O_{(s)}$ after reaction with PO_4, which is consistent with model results (Fig. 3a-b). Excess $La_2(CO_3)_3{\cdot}8H_2O_{(s)}$ was stable under these experimental conditions. In Fig. 4, traces b-d, the broad regions at 2θ values of ~29° and ~ 31° that are not present in Fig. 4, trace a provide direct evidence for the formation of $LaPO_4{\cdot}nH_2O_{(s)}$ (XRD peaks marked with green stars). Because major $La(OH)_{3(s)}$ peaks appear at similar 2θ as peaks from $La_2(CO_3)_3{\cdot}8H_2O_{(s)}$ and $LaCO_3OH_{(s)}$ (Fig. 4, trace c), it is difficult to confirm by XRD the presence of $La(OH)_{3(s)}$ in the high pH sample as predicted by thermodynamic modeling. Interestingly, XRD revealed that the starting material contained a $LaCO_3OH_{(s)}$ phase (Fig. 4, trace a) that persisted after reactions with PO_4 (Fig. 4, traces b-e). $LaCO_3OH_{(s)}$ is not included in the Visual MINTEQ database, and thermodynamic parameters are absent from the literature. We assume that $LaCO_3OH_{(s)}$ was not an important phase in our system because experimental data from batch tests closely matched modeling predictions.

To further confirm $LaPO_{4(s)}$ as a reaction product, an additional equilibrium batch experiment was performed with $La_2(CO_3)_3{\cdot}8H_2O_{(s)}$ at an initial molar P/La = 2:1. As shown in Fig. 4, trace e, $La_2(CO_3)_3{\cdot}8H_2O_{(s)}$ was depleted in the system with excess PO_4, and the resultant product was $LaPO_4{\cdot}nH_2O_{(s)}$, which confirms that PO_4 removal occurred predominantly by precipitation. It is consistent with previous studies describing PO_4 removal by La-exchanged bentonite (Dithmer et al., 2015; Slade and Gates, 1999) and $La(OH)_3$-modified polyacrylonitrile nanofibers (He et al., 2015) and wheat straws (Qiu et al., 2017). Due to the similarities in XRD peak positions for hydrous and anhydrous $LaPO_4$, it was not possible to rule out of the presence of anhydrous $LaPO_{4(s)}$ in these products; however, the pattern of peak intensities most closely resembles $LaPO_4{\cdot}0.5H_2O_{(s)}$. The XRD pattern of $LaPO_{4(s)}$ synthesized from $La_2(CO_3)_3{\cdot}8H_2O_{(s)}$ exhibited broad peaks (Fig. 4, trace e), suggesting that this phase has a small particle size and/or low crystallinity.

To provide further insight into the PO_4-removal process, the formation and growth processes of $LaPO_{4(s)}$ during our kinetic experiment (Fig. 5) were investigated by characterizing particles formed at different contact

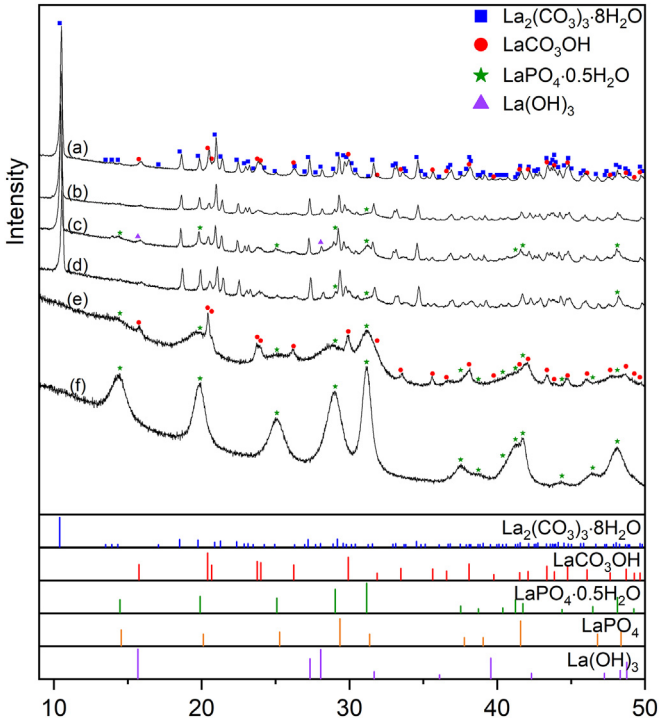

Fig. 4. X-ray diffraction patterns (traces a-f) of (a) the $La_2(CO_3)_3{\cdot}8H_2O_{(s)}$ starting material; (b) and (c) products formed by reacting $La_2(CO_3)_3{\cdot}8H_2O_{(s)}$ with PO_4 at a molar P:La ratio of 1:2 in UPW at pH 7 and 12, respectively; (d) products formed by reacting $La_2(CO_3)_3{\cdot}8H_2O_{(s)}$ with PO_4 in wastewater at a molar P:La ratio of 1:2; (e) $LaPO_{4(s)}$ formed by reacting $La_2(CO_3)_3{\cdot}8H_2O_{(s)}$ with PO_4 in UPW at pH 7 at a molar P:La ratio of 2:1, (f) $LaPO_{4(s)}$ formed by reacting $LaCl_3{\cdot}7H_2O$ with PO_4 in UPW at a molar P:La ratio of 2:1. Note that colored dots indicating peaks corresponding to the $La_2(CO_3)_3{\cdot}8H_2O_{(s)}$ and $LaCO_3OH_{(s)}$ are omitted from (b), (c), and (d) for clarity. The reference patterns obtained from powder diffraction files are plotted below for $La_2(CO_3)_3{\cdot}8H_2O$ (card no. 04–010-3609), $LaCO_3OH$ (card no. 00–049-0981), $LaPO_4$ (card no. 00–004-0635), $LaPO_4$ 0.5 H_2O (card no. 00–046-1439), and $La(OH)_3$ (card no. 01–083-4962).

times using STEM-EDS. The starting $La_2(CO_3)_{3(s)}$ material possessed a rod-like morphology, with La evenly distributed along the rod (Fig. S5). When exposed to PO_4, the surface of the $La_2(CO_3)_{3(s)}$ particle became etched, with P distributed at the edges (Fig. 5b-c). The inner rod structure began to collapse, but the particles still maintained their outer shape. As the reaction progressed, smaller particles with less well-defined shape were found adhering to the surface of the particles, and $La_2(CO_3)_{3(s)}$ was disappeared (Fig. 5d-e). Meanwhile, small, villous $LaPO_{4(s)}$ particles appeared in the solution (Fig. 5a; shown at higher magnification after equilibrium is reached in Fig. 5f-g). Within the newly formed particles, La and P were distributed homogenously. STEM images of intermediate states (Fig. 5a) suggest that $LaPO_{4(s)}$ was formed on the surface of $La_2(CO_3)_{3(s)}$ particles as well as in the solution. Thus, both heterogeneous nucleation [$LaPO_{4(s)}$ formation on the surface of $La_2(CO_3)_{3(s)}$] and homogeneous nucleation [$LaPO_{4(s)}$ formation by reaction of PO_4 with La^{3+} in bulk solution] appear to play a role. The latter reaction may become more important as pH decreased with concomitantly increased reaction rates, as demonstrated by the kinetic data (Fig. 6).

3.5. pH-dependent PO_4 removal rates with $La_2(CO_3)_{3(s)}$

Lack of consistency between measured $TOTPO_{4(aq)}$ and model predictions between pH 10–12 displayed in Fig. 3a was attributed to pH-dependent kinetics; thus, we further explored PO_4 removal kinetics with $La_2(CO_3)_{3(s)}$. Batch kinetic experiments conducted between pH 4 and 12 indicated that the rate of PO_4 removal was pH-dependent (Fig. 6). The time required for $La_2(CO_3)_{3(s)}$ to remove $TOTPO_{4(aq)}$ to below the reporting limit increased by two orders of magnitude from 11 h at pH 4 to ~1000 h at pH 12. Across this pH range, the ligands PO_4^{3-}, CO_3^{2-}, and OH^- compete for La^{3+}. We hypothesize that the high rate of PO_4 precipitation with La^{3+} contributed to enhanced dissolution of $La_2(CO_3)_{3(s)}$ in the pH 4–7 range. As the pH increased, the concentration of both OH^- and CO_3^{2-} increased, decreasing the rate of $La_2(CO_3)_{3(s)}$ dissolution and thus the reactant concentration for $LaPO_{4(s)}$ formation.

3.6. Phosphate removal from wastewater

We conducted equilibrium experiments in wastewater (pH 7 and 25 °C, same conditions as in UPW) to assess the selectivity of $La_2(CO_3)_{3(s)}$ for PO_4 in a complex matrix (Fig. S14). Equilibrium experiments with different initial PO_4 concentrations in UPW largely overlapped with the wastewater experiments, suggesting negligible matrix effects when equilibrium conditions are reached (Fig. S14). Kinetic data shown in Fig. S15 suggested that even though the reaction rate was retarded in wastewater relative to UPW, PO_4 was removed to below the reporting limit. The effect of interfering ions (e.g., SO_4^{2-}, NO_3^-, CO_3^{2-}, and dissolved organic matter) on reducing the overall rate constant for PO_4 removal by a La-containing resin was observed in previous studies (Zhang et al., 2012a, 2016). One possible reason for changes in removal rates is that competing ions delay formation of $LaPO_{4(s)}$ nanocrystals (Zhang et al., 2016).

Visual MINTEQ results showed that major ions (e.g., SO_4^{2-}, Ca^{2+}, Mg^{2+}, NO_3^-, Cl^-, Na^+, K^+ and F^-) in wastewater have a negligible impact on $LaPO_{4(s)}$ precipitation at equilibrium (Fig. S16), which is consistent with prior studies using La-containing materials (Chen et al., 2016; Dong et al., 2017; Huang et al., 2014a; Wu et al., 2007, 2017). The selectivity of La for PO_4 can be attributed to the low solubility of $LaPO_{4(s)}$ relative to other possible La-based solids containing ligands other than PO_4. As indicated in Fig. S16, the presence of Ca^{2+} (0.40 mM) may improve PO_4 removal in systems containing La because hydroxyapatite [$Ca_5(PO_4)_3OH_{(s)}$] forms at pH > 12.3 (conditions, at which PO_4 removal by La is kinetically hindered; Fig. 4) and binds additional PO_4. Conversely, a negligible impact was predicted for Mg^{2+}, F^-, and Cl^- (results not shown) over the entire pH range. Even though Ca^{2+} and Mg^{2+} can precipitate PO_4, and F^- can react with La^{3+} to form $LaF_{3(s)}$, model results illustrated that La^{3+} preferentially reacts with PO_4 at environmentally relevant pH values.

In a separate scenario (model results shown in Fig. S17), carbonate (5 mM of CO_3^{2-}) enhances the stability of $La_2(CO_3)_{3(s)}$ over a wider pH range (pH 5.3–11.3) than in the absence of CO_3^{2-} (Fig. S17a). In an open system (atmospheric CO_2 pressure, 0.00038 atm), dissolution of $La_2(CO_3)_{3(s)}$ commences at pH 6.5, compared to pH 5.5 in a closed system (Fig. S17b). The latter results also illustrate that the carbonate system impacts the pH-dependent solubility of La, as discussed below.

3.7. Minimizing release of soluble La during PO_4 sequestration

As shown in Fig. 1, dissolution of $La_2(CO_3)_{3(s)}$ and $La(OH)_{3(s)}$ in UPW occurred at pH < 5.5 and < 8.0, respectively. To further investigate La solubilization under different scenarios, we predicted $TOTLa_{(aq)}$ in equilibrium with $La(OH)_{3(s)}$, $La_2(CO_3)_{3(s)}$, and $LaPO_{4(s)}$ as a function of pH, initial dissolved inorganic carbon (DIC) to reflect alkalinity, and initial dose of the La-containing material. $TOTLa_{(aq)}$ results in UPW (pH 6.0–8.5 range) are shown in Fig. 7. $TOTLa_{(aq)}$ in equilibrium with the La-containing solids increased in the order $LaPO_{4(s)} < La_2(CO_3)_{3(s)} < La(OH)_{3(s)}$. Compared to a concentration that has been deemed acceptable from an ecotoxicity perspective (2.9×10^{-8} M) (Herrmann et al., 2016), $TOTLa_{(aq)}$ concentrations exceeded that level with both $La_2(CO_3)_{3(s)}$ and $La(OH)_{3(s)}$ for pH 6.0–8.5. In the presence of DIC (1 or 10 mM), La leaching from $La(OH)_{3(s)}$ and $La_2(CO_3)_{3(s)}$ decreased because of $La_2(CO_3)_{3(s)}$ precipitation. Predicted $TOTLa_{(aq)}$ in equilibrium with $La_2(CO_3)_{3(s)}$ was below the PNEC for pH 7.2–9.3 with 10 mM of DIC. In the presence of PO_4, model predictions of $TOTLa_{(aq)}$ in equilibrium with excess $LaPO_{4(s)}$ remained below the PNEC for pH > 4.5. However, La solubilization from $LaPO_{4(s)}$ can increase in water with elevated DIC as a result of $La(CO_3)_2^-$, $LaCO_3^+$, and $LaHCO_3^{2+}$ complex formation,

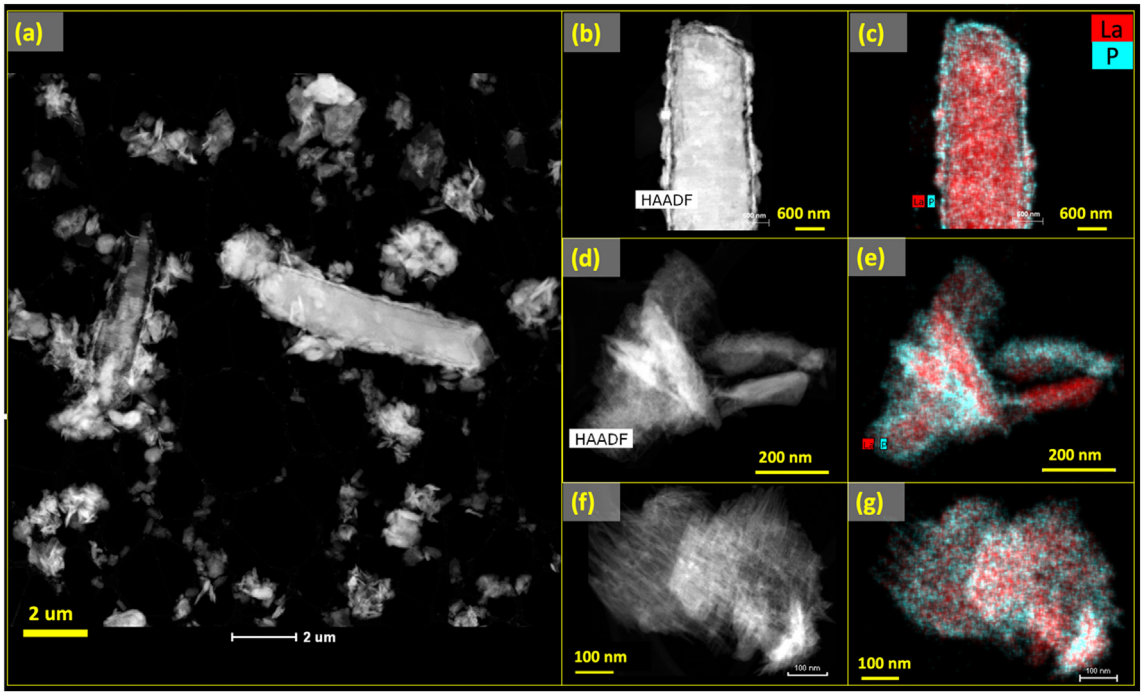

Fig. 5. TEM images for a system, in which $La_2(CO_3)_{3(s)}$ (1.62 mM) reacted with NaH_2PO_4 (1.62 mM, La:P = 2:1) at pH 7 and 25 °C. EDS mapping and morphologies of particles in the system: (a) intermediate state of PO_4-removal by $La_2(CO_3)_{3(s)}$ (contact time: 5.5 h), (b) and (c) upper half of a single $La_2(CO_3)_{3(s)}$ particle in a PO_4 solution (contact time: 2 min), (d) and (e) $La_2(CO_3)_{3(s)}$ particles in a PO_4 solution (contact time: 5.5 h), (f) and (g) $LaPO_{4(s)}$ particle (contact time: 50.5 h). To confirm that particles are representative, corresponding EDS mapping and spectra are provided in Figs. S6 - S13.

especially in the pH 8–12 range. The concentration of the dosed La-containing material (0.001 mM - 8 mM of La) had a negligible effect on $TOTLa_{(aq)}$ for $LaPO_{4(s)}$, but $TOTLa_{(aq)}$ increased when pH is <7 for $La_2(CO_3)_{3(s)}$ and < 8.5 for $La(OH)_{3(s)}$ (Fig. S18).

3.8. Study limitations

Our study determined that $La_2(CO_3)_{3(s)}$ removed PO_4 from solution by precipitation of $LaPO_4$ solids. The 1:1 P:La solid phase ratio seen in this study is also observed in many other studies. Although it is tempting to suggest that precipitation is the dominant mechanism in all of these studies as well, other removal mechanisms are possible. For example, advanced materials may be generated such that all La atoms in the solid are available for sorption (Min et al., 2019). In many cases, revisiting the specific experimental system with spectroscopic, microscopic, or scattering interrogation of the solid phase may be required for definitive assignment of mechanism.

An additional limitation of this study is that we could not directly determine $LaPO_{4(s)}$ formation at low dissolved PO_4 concentrations because the quantity of $LaPO_{4(s)}$ formed would have been insufficient for our characterization techniques. It is possible that adsorption may predominate over precipitation at very low dissolved PO_4 concentrations. However, Visual MINTEQ calculations showed that in the presence of $La_2(CO_3)_{3(s)}$, $LaPO_{4(s)}$ can be formed at PO_4 concentration as low as 10^{-14} M, even when La_2

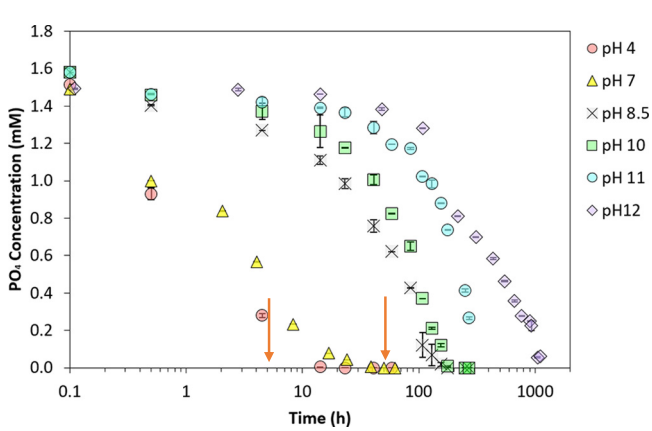

Fig. 6. Solution pH-dependent PO_4 removal kinetics in batch reactors containing 1.62 mM $La_2(CO_3)_{3(s)}$ and 1.62 mM of NaH_2PO_4 at 25 °C. Arrows indicate sampling times for Fig. 5 (5.5 h at pH 7 for Fig. 5a and 50.5 h at pH 7 for Fig. 5f and g).

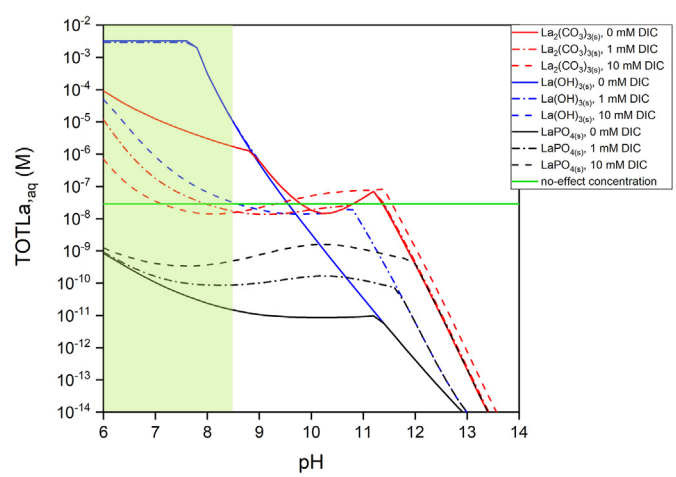

Fig. 7. Dependence of $TOTLa_{(aq)}$ on solution pH. Visual MINTEQ results for solutions dosed with 3.24 mM of $La(OH)_{3(s)}$ or $LaPO_{4(s)}$, or 1.62 mM of $La_2(CO_3)_{3(s)}$ as a finite solid as a function of pH (6–14) and dissolved inorganic carbon (DIC) addiction of 0, 1 or 10 mM (simulated by adding CO_3 to the system) at 25 °C. The green line represents the La^{3+} concentration that is considered to have no ecotoxicological effect in freshwater systems (2.88×10^{-8} M). Shaded green region highlights the environmentally relevant pH range of 6.0–8.5.

$(CO_3)_{3(s)}$ is dosed at μM concentrations (Fig. S19) suggesting that precipitation is possible even in waters with low dissolved P.

In addition, it has been reported that the presence of dissolved organic matter (DOM) interferes with $LaPO_{4(s)}$ formation (Zhi et al., 2020, 2021). DOM contains relatively strong acidic (pKa of 3.3–4.0) and weak acidic groups (pKa > 6), as well as a few bidentate sites (pKa of 4–16) that may act as major competitor ligands for La (Sonke and Salters, 2006; Tipping and Hurley, 1992). Therefore, in wastewater containing high concentrations of DOM, the PO4 removal efficiency by La-containing materials may be reduced.

4. Conclusion and environmental implications

Numerous La-containing materials have been developed for capturing aqueous PO_4 species in complex matrices. Based on results from geochemical simulations, batch equilibrium and kinetic experiments, and reaction product characterization, our results indicate that precipitation of $LaPO_{4(s)}$ was the primary mechanism of PO_4 removal in our systems. Such understanding is critical for the development of La-containing materials for PO_4 removal. Based on the precipitation mechanism, the maximum PO_4 uptake follows the stoichiometry of P:La = 1:1. Importantly, from an ecotoxicological perspective, our results suggest that La^{3+} solubilization is lower with $La_2(CO_3)_{3(s)}$ than with $La(OH)_{3(s)}$, especially in low-alkalinity water. This study also highlights the high affinity of $La_2(CO_3)_{3(s)}$ for PO_4 in the presence of competing anions in wastewater. Nevertheless, due to the insoluble nature of $LaPO_{4(s)}$, recovery and reuse of PO_4 or La from $LaPO_{4(s)}$ is expected to be difficult; future research is needed to explore an efficient and effective way to extract PO_4 from La materials.

CRediT authorship contribution statement

The manuscript was written through the contributions of all authors. All authors have approved the final version of the manuscript.

Declaration of competing interest

The authors declare that they have no known competing financial interests or personal relationships that could have appeared to influence the work reported in this paper.

Acknowledgments

This work was supported by the Game-Changing Research Initiative Program (GRIP) through the NC State Office of Research and Innovation (ORI), RTI International, and the Kenan Institute for Engineering, Science and Technology. This work was supported by the USDA National Institute of Food and Agriculture, Hatch project NC02713. STEM and XRD analyses were performed at the Analytical Instrumentation Facility (AIF) of North Carolina State University, which is supported by the State of North Carolina and the National Science Foundation (award number ECCS-2025064). We thank Josh Russell, Dr. Lisa Castellano, Dr. Ching-Chang Chung, Dr. Yang Liu, Dr. Zihong Fan, Lan Chen, Yao Luo, and Priscyla Marquez for laboratory assistance.

Appendix A. Supplementary data

Supplementary data to this article can be found online at https://doi.org/10.1016/j.scitotenv.2022.153153.

References

Barry, M.J., Meehan, B.J., 2000. The acute and chronic toxicity of lanthanum to Daphnia carinata. Chemosphere 41, 1669–1674.

Chen, L., Liu, F., Wu, Y., Zhao, L., Li, Y., Zhang, X., Qian, J., 2018. In situ formation of $La(OH)_3$-poly(vinylidene fluoride) composite filtration membrane with superior phosphate removal properties. Chem. Eng. J. 347, 695–702.

Chen, M., Huo, C., Li, Y., Wang, J., 2016. Selective adsorption and efficient removal of phosphate from aqueous medium with graphene-lanthanum composite. ACS Sustain. Chem. Eng. 4, 1296–1302.

Cheng, R., Shen, L.J., Zhang, Y.Y., Dai, D.Y., Zheng, X., Liao, L.W., Wang, L., Shi, L., 2018. Enhanced phosphate removal fromwater by honeycomb-like microporous lanthanum- chitosan magnetic spheres. Water (Switzerland) 10.

Conley, D.J., Paerl, H.W., Howarth, R.W., Boesch, D.F., Seitzinger, S.P., Havens, K.E., Lancelot, C., Likens, G.E., 2009. Ecology - controlling eutrophication: nitrogen and phosphorus. Science (80-.) 323, 1014–1015.

Copetti, D., Finsterle, K., Marziali, L., Stefani, F., Tartari, G., Douglas, G., Reitzel, K., Spears, B.M., Winfield, I.J., Crosa, G., D'Haese, P., Yasseri, S., Lürling, M., 2016. Eutrophication management in surface waters using lanthanum modified bentonite: a review. Water Res. 97, 162–174.

Das, T., Sharma, A., Talukder, G., 1988. Effects of lanthanum in cellular systems. Biol. Trace Elem. Res. 18, 201–228.

Davis, J.A., 1990. Surface complexation modeling in aqueous geochemistry. Miner. Interface Geochemistry. 23, pp. 177–259.

Dithmer, L., Lipton, A.S., Reitzel, K., Warner, T.E., Lundberg, D., Nielsen, U.G., 2015b. Characterization of phosphate sequestration by a lanthanum modified bentonite clay: a solid-state NMR, EXAFS, and PXRD study. Environ. Sci. Technol. 49, 4559–4566.

Dithmer, L., Nielsen, U.G., Lürling, M., Spears, B.M., Yasseri, S., Lundberg, D., Moore, A., Jensen, N.D., Reitzel, K., 2016. Responses in sediment phosphorus and lanthanum concentrations and composition across 10 lakes following applications of lanthanum modified bentonite. Water Res. 97, 101–110.

Dong, S., Wang, Y., Zhao, Y., Zhou, X., Zheng, H., 2017. La3 + /La(OH)3 loaded magnetic cationic hydrogel composites for phosphate removal: effect of lanthanum species and mechanistic study. Water Res. 126, 433–441.

Douglas, G.B., 2002. Remediation Material And Remediation Process for Sediments.

Douglas, G.B., Adeney, J.A., Robb, M., 1999. A novel technique for reducing bioavailable phosphorus in water and sediments. International Association Water Quality Conference on Diffuse Pollution.

Douglas, G.D., Adeney, J.A., Zappia, L.R., 2000. Sediment remediation project: 1998/9 laboratory trial report CSIRO land and water. Commonw. Sci. Ind. Res. Organ.

Du, H., Lung, C.Y.K., Lau, T.C., 2018. Efficient adsorption, removal and recovery of phosphate and nitrate from water by a novel lanthanum(III)-dowex M4195 polymeric ligand exchanger. Environ. Sci. Water Res. Technol. 4, 421–427.

Dzombak, D.A., Morel, F.M.M., 1990. Surface Complexation Modeling: Hydrous Ferric Oxide. John Wiley & Sons.

Emmanuelawati, I., Yang, J., Zhang, J., Zhang, H., Zhou, L., Yu, C., 2013. Low-cost and large-scale synthesis of functional porous materials for phosphate removal with high performance. Nanoscale 5, 6173–6180.

Fang, L., Shi, Q., Nguyen, J., Wu, B., Wang, Z., Lo, I.M.C., 2017. Removal mechanisms of phosphate by lanthanum hydroxide nanorods: investigations using EXAFS, ATR-FTIR, DFT, and surface complexation modeling approaches. Environ. Sci. Technol. 51, 12377–12384.

Fang, L., Liu, R., Li, J., Xu, C., Huang, L.-Z.Z., Wang, D., 2018. Magnetite/lanthanum hydroxide for phosphate sequestration and recovery from lake and the attenuation effects of sediment particles. Water Res. 130, 243–254.

Field, H.R., Whitaker, A.H., Henson, J.A., Duckworth, O.W., 2019. Sorption of copper and phosphate to diverse biogenic iron (oxyhydr)oxide deposits. Sci. Total Environ. 697, 134111.

Gonzalez, V., Vignati, D.A.L., Leyval, C., Giamberini, L., 2014. Environmental fate and ecotoxicity of lanthanides: are they a uniform group beyond chemistry? Environ. Int. 71, 148–157.

Gustafsson, J.P., 2011. Visual MINTEQ 3.0 User Guide. KTH, Dep. L. Water Resources, Stock, Sweden.

He, J., Wang, W., Sun, F., Shi, W., Qi, D., Wang, K., Shi, R., Cui, F., Wang, C., Chen, X., 2015. Highly efficient phosphate scavenger based on well-dispersed La(OH)3 nanorods in polyacrylonitrile nanofibers for nutrient-starvation antibacteria. ACS Nano 9, 9292–9302.

Herrmann, H., Nolde, J., Berger, S., Heise, S., 2016. Aquatic ecotoxicity of lanthanum - a review and an attempt to derive water and sediment quality criteria. Ecotoxicol. Environ. Saf. 124, 213–238.

Huang, C.-H., 2011. Rare Earth Coordination Chemistry: Fundamentals And Applications. John Wiley & Sons.

Huang, W., Zhu, Y., Tang, J., Yu, X., Wang, X., Li, D., Zhang, Y., 2014. Lanthanum-doped ordered mesoporous hollow silica spheres as novel adsorbents for efficient phosphate removal. J. Mater. Chem. A 2, 8839.

Huang, W., Yu, X., Tang, J., Zhu, Y., Zhang, Y., Li, D., 2015. Enhanced adsorption of phosphate by flower-like mesoporous silica spheres loaded with lanthanum. Microporous Mesoporous Mater. 217, 225–232.

Huang, W.-Y., Li, D., Liu, Z.-Q.Q., Tao, Q., Zhu, Y., Yang, J., Zhang, Y.-M.M., 2014. Kinetics, isotherm, thermodynamic, and adsorption mechanism studies of $La(OH)_3$-modified exfoliated vermiculites as highly efficient phosphate adsorbents. Chem. Eng. J. 236, 191–201.

Jia, X., He, X., Han, K., Ba, Y., Zhao, X., Zhang, Q., 2019. La_2O_3-modified MCM-41 for efficient phosphate removal synthesized using natural diatomite as precursor. Water Sci. Technol. 9, 1878–1886.

Kong, L., Tian, Y., Li, N., Liu, Y., Zhang, J.J., Zhang, J.J., Zuo, W., 2018. Highly-effective phosphate removal from aqueous solutions by calcined nano-porous palygorskite matrix with embedded lanthanum hydroxide. Appl. Clay Sci. 162, 507–517.

Lai, L., Xie, Q., Chi, L., Gu, W., Wu, D., 2016. Adsorption of phosphate from water by easily separable Fe_3O_4@SiO_2 core/shell magnetic nanoparticles functionalized with hydrous lanthanum oxide. J. Colloid Interface Sci. 465, 76–82.

Lin, J., Zhao, Y., Zhang, Z.Z., Zhan, Y., Zhang, Z.Z., Wang, Y., Yu, Y., Wu, X., 2019. Immobilization of mobile and bioavailable phosphorus in sediments using lanthanum hydroxide and magnetite/lanthanum hydroxide composite as amendments. Sci. Total Environ. 687, 232–243.

Liu, J., Wan, L., Zhang, L., Zhou, Q., 2011. Effect of pH, ionic strength, and temperature on the phosphate adsorption onto lanthanum-doped activated carbon fiber. J. Colloid Interface Sci. 364, 490–496.

Liu, J., Zhou, Q., Chen, J., Zhang, L., Chang, N., 2013. Phosphate adsorption on hydroxyl-iron-lanthanum doped activated carbon fiber. Chem. Eng. J. 215, 859–867.

Mayer, B.K., Baker, L.A., Boyer, T.H., Drechsel, P., Gifford, M., Hanjra, M.A., Parameswaran, P., Stoltzfus, J., Westerhoff, P., Rittmann, B.E., 2016. Total value of phosphorus recovery. Environ. Sci. Technol. 50, 6606–6620.

Min, X., Wu, X., Shao, P., Ren, Z., Ding, L., Luo, X., 2019. Ultra-high capacity of lanthanum-doped UiO-66 for phosphate capture: unusual doping of lanthanum by the reduction of coordination number. Chem. Eng. J. 358, 321–330.

Mucci, M., Douglas, G., Lürling, M., 2020. Lanthanum modified bentonite behaviour and efficiency in adsorbing phosphate in saline waters. Chemosphere 249, 1–10.

Park, Y., Gorman, C., Ford, E., 2020. Lanthanum carbonate nanofibers for phosphorus removal from water. J. Mater. Sci. 55, 5008–5020.

Pokrovsky, O.S., Schott, J., 2002. Surface chemistry and dissolution kinetics of divalent metal carbonates. Environ. Sci. Technol. 36, 426–432.

Qiu, H., Liang, C., Yu, J., Zhang, Q., Song, M., Chen, F., 2017. Preferable phosphate sequestration by nano-La(III) (hydr)oxides modified wheat straw with excellent properties in regeneration. Chem. Eng. J. 315, 345–354.

Rashidi Nodeh, H., Sereshti, H., Zamiri Afsharian, E., Nouri, N., 2017. Enhanced removal of phosphate and nitrate ions from aqueous media using nanosized lanthanum hydrous doped on magnetic graphene nanocomposite. J. Environ. Manag. 197, 265–274.

Reitzel, K., Andersen, F.T.Ø., Egemose, S., Jensen, H.S., 2013. Phosphate adsorption by lanthanum modified bentonite clay in fresh and brackish water. Water Res. 47, 2787–2796.

Reitzel, K., Balslev, K.A., Jensen, H.S., 2017. The influence of lake water alkalinity and humic substances on particle dispersion and lanthanum desorption from a lanthanum modified bentonite. Water Res. 125, 191–200.

Rentz, J.A., Turner, I.P., Ullman, J.L., 2009. Removal of phosphorus from solution using biogenic iron oxides. Water Res. 43, 2029–2035.

Robb, M., Greenop, B., Goss, Z., Douglas, G., Adeney, J., 2003. Application of PhoslockTM, an innovative phosphorus binding clay, to two Western Australian waterways: preliminary findings. Hydrobiologia 237–243.

Roy, S.K., Sengupta, P.K., 1988. Electrical properties and the surface characteristics of lanthanum oxide/water interface. J. Colloid Interface Sci. 125, 340–343.

Shin, E.W., Karthikeyan, K.G., Tshabalala, M.A., 2005. Orthophosphate sorption onto lanthanum-treated lignocellulosic sorbents. Environ. Sci. Technol. 39, 6273–6279.

Slade, P.G., Gates, W.P., 1999. Comments on the exchange of La3+ by Na+ and K+ in Lavermiculites and smectites and the precipitation of Rhabdophane (LaPO4• H2O). CSIRO L. Water Report.

Sonke, J.E., Salters, V.J.M., 2006. Lanthanide–humic substances complexation. I. Experimental evidence for a lanthanide contraction effect. Geochim. Cosmochim. Acta 70 (6), 1495–1506.

Sowers, T.D., Harrington, J.M., Polizzotto, M.L., Duckworth, O.W., 2017. Sorption of arsenic to biogenic iron (oxyhydr)oxides produced in circumneutral environments. Geochim. Cosmochim. Acta 198, 194–207.

Sposito, G., 2004. The Surface Chemistry of Natural Particles. Oxford University Press on Demand.

Tang, Q., Shi, C., Shi, W., Huang, X., Ye, Y., Jiang, W., Kang, J., Liu, D., Ren, Y., Li, D., 2019. Preferable phosphate removal by nano-La(III) hydroxides modified mesoporous rice husk biochars: role of the host pore structure and point of zero charge. Sci. Total Environ. 662, 511–520.

Tipping, E, Hurley, M.A, 1992. A unifying model of cation binding by humic substances. Geochim. Cosmochim. Acta 56 (10), 3627–3641.

Veith, J.A., Sposito, G., 1977. On the use of the langmuir equation in the interpretation of "Adsorption" phenomena 1. Soil Sci. Soc. Am. J. 41, 697–702.

Waajen, G., van Oosterhout, F., Douglas, G., Lürling, M., 2016. Management of eutrophication in Lake De kuil (The Netherlands) using combined flocculant – lanthanum modified bentonite treatment. Water Res. 97, 83–95.

Weiner, E.R., 2008. Applications of Environmental Aquatic Chemistry: A Practical Guide. CRC Press.

Wu, B., Fang, L., Fortner, J.D., Guan, X., Lo, I.M.C., 2017. Highly efficient and selective phosphate removal from wastewater by magnetically recoverable $La(OH)_3/Fe_3O_4$ nanocomposites. Water Res. 126, 179–188.

Wu, R., Lam, K., Lee, J.M.N.N., Lau, T.C.C., 2007. Removal of phosphate from water by a highly selective La(III)-chelex resin. Chemosphere 69, 289–294.

Wu, Y., Li, X., Yang, Q., Wang, D., Xu, Q., Yao, F., Chen, F., Tao, Z., Huang, X., 2019. Hydrated lanthanum oxide-modified diatomite as highly efficient adsorbent for low-concentration phosphate removal from secondary effluents. J. Environ. Manag. 231, 370–379.

Wu, Wan, J., Zhang, Y., Pan, B.-C., Lo, I.M.C., 2019. Selective phosphate removal from water and wastewater using sorption: process fundamentals and removal mechanisms. Environ. Sci. Technol. 54, 50–66.

Xie, J., Wang, Z., Fang, D., Li, C., Wu, D., 2014. Green synthesis of a novel hybrid sorbent of zeolite/lanthanum hydroxide and its application in the removal and recovery of phosphate from water. J. Colloid Interface Sci. 423, 13–19.

Xu, R., Zhang, M., Mortimer, R.J.G.G., Pan, G., 2017. Enhanced phosphorus locking by novel lanthanum/aluminum-hydroxide composite: implications for eutrophication control. Environ. Sci. Technol. 51, 3418–3425.

Yang, J., Zhou, L., Zhao, L., Zhang, H., Yin, J., Wei, G., Qian, K., Wang, Y., Yu, C., 2011. A designed nanoporous material for phosphate removal with high efficiency. J. Mater. Chem. 21, 2489–2494.

Yang, J., Yuan, P., Chen, H.-Y., Zou, J., Yuan, Z., Yu, C., 2012. Rationally designed functional macroporous materials as new adsorbents for efficient phosphorus removal. J. Mater. Chem. 22, 9983–9990.

Yu, J., Xiang, C., Zhang, G., Wang, H., Ji, Q., Qu, J., 2019. Activation of lattice oxygen in LaFe (oxy)hydroxides for efficient phosphorus removal. Environ. Sci. Technol. 53, 9073–9080.

Yuan, L., Qiu, Z., Lu, Y., Tariq, M., Yuan, L., Yang, J., Li, Z., Lyu, S., 2018. Development of lanthanum hydroxide loaded on molecular sieve adsorbent and mechanistic study for phosphate removal. J. Alloys Compd. 768, 953–961.

Zhang, J., Shen, Z., Shan, W., Mei, Z., Wang, W., 2011. Adsorption behavior of phosphate on lanthanum(III)-coordinated diamino-functionalized 3D hybrid mesoporous silicates material. J. Hazard. Mater. 186, 76–83.

Zhang, L., Liu, J., Wan, L., Zhou, Q., Wang, X., 2012a. Batch and fixed-bed column performance of phosphate adsorption by lanthanum-doped activated carbon fiber. Water Air Soil Pollut. 223, 5893–5902.

Zhang, L., Zhou, Q., Liu, J., Chang, N., Wan, L., Chen, J., 2012b. Phosphate adsorption on lanthanum hydroxide-doped activated carbon fiber. Chem. Eng. J. 185, 160–167.

Zhang, X., Wang, W., Dai, S., Cui, F., 2018. Synchronous, efficient and fast removal of phosphate and organic matter by carbon-coated lanthanum nanorods. RSC Adv. 8, 11754–11763.

Zhang, Y., Pan, B., Shan, C., Gao, X., 2016. Enhanced phosphate removal by nanosized hydrated La(III) oxide confined in cross-linked polystyrene networks. Environ. Sci. Technol. 50, 1447–1454.

Zhi, Y., Zhang, C., Hjorth, R., Baun, A., Duckworth, O.W., Call, D.F., Knappe, D.R.U., Jones, J.L., Grieger, K., 2020. Emerging lanthanum (III)-containing materials for phosphate removal from water: a review towards future developments. Environ. Int. 145, 106115.

Zhi, Y., Call, D.F., Grieger, K.D., Duckworth, O.W., Jones, J.L., Knappe, D.R.U., 2021. Influence of natural organic matter and pH on phosphate removal by and filterable lanthanum release from lanthanum-modified bentonite. Water Res. 202, 117399.